ELSEVIER

Biochimica et Biophysica Acta 1321 (1997) 165–178

BIOCHIMICA ET BIOPHYSICA ACTA
BBA

Investigations of Chl *a* aggregates cross-linked by dioxane in 3-methylpentane

J.A.I. Oksanen [a,*], E.I. Zenkevich [b], V.N. Knyukshto [b], S. Pakalnis [c], P.H. Hynninen [d], J.E.I. Korppi-Tommola [a]

[a] *Department of Physical Chemistry, University of Jyväskylä, P.O. Box 35, FIN-40351 Jyväskylä, Finland*
[b] *Institute of Molecular and Atomic Physics, Academy of Science of Belarus, F. Skaryna Ave. 70, Minsk 220072, Belarus*
[c] *Institute of Physics, A. Gostanto 12, 2600 Vilnius, Lithuania*
[d] *Department of Chemistry, University of Helsinki, P.O. Box 55, 00014 Helsinki, Finland*

Received 14 November 1996; revised 25 March 1997; accepted 9 April 1997

Abstract

In this work, dioxane-bound aggregates of chlorophyll a are prepared in 3-methylpentane. The properties of the aggregates are studied by using steady-state and time-resolved spectroscopies. The Q_y-region absorption spectrum of the chlorophyll *a*-dioxane aggregate shows four clearly resolvable narrow bands with comparable intensities. The band maxima are located at 683, 689, 698 and 702 nm. The emission spectrum consists of two emission bands centred at 699 and 702 nm suggesting the presence of two types of aggregates. High degree of fluorescence polarization is detected yielding the angles between the absorption transition moments with respect to the 702 nm emission transition moment. The circular dichroism signal is strong and the sign sequence follows that of the polarization spectrum. ψ-type effect is discovered due to long-range interactions within the sizable aggregate frame. The insensitivity of the time-resolved emission kinetics to the temperature indicate the excitation delocalization length to be short. The rapid loss of time-resolved anisotropy at certain wavelengths supports the energy transfer to take place. The independence of the excitation spectrum over a broad range of emission wavelengths suggests that the two diverse spectral types are found within the same macro-aggregate and that they are coupled together by the energy transfer. © 1997 Elsevier Science B.V.

Keywords: Dioxane aggregate; Chlorophyll *a*; Excitation delocalization; Fluorescence polarization; ψ-type circular dichroism; Single-photon counting

1. Introduction

The investigations of the primary light-harvesting reactions in natural photosynthetic systems have improved appreciably our understanding of the mechanisms involved in the transfer and trapping of solar energy. Steady-state and time-resolved fluorescence measurements and absorption spectroscopy have served as important methods in these studies [1–5]. The light-harvesting photosynthetic antenna-complexes are responsible for the light absorption and the efficient energy transfer to the reaction centres. In the reaction centre, the excitation energy is transformed into the form of a long-lived charge separation. The flow of excitation energy in the antenna is principally

* Corresponding author. Fax: +358 14-602551; E-mail: jaijo@dodo.jyu.fi

PII S0005-2728(97)00038-8

determined by mutual distances and orientations between the interacting antenna chromophores. However, the exact mechanism of the energy transfer and the pigment organization in the light-harvesting antennae of bacteria and plants still remain to some extent unknown.

The interpretation of the spectral-kinetic parameters of the in vivo photosynthetic light-harvesting systems is met with considerable difficulties. Even small amounts of impurities remaining in the sample after the isolation procedure, can change the spectral and kinetic properties of the antennae dramatically. Also the role of the apoproteins is often unknown. The extent to which the structure of the light-harvesting system is determined only by the pure mutual interactions between the pigments, is usually left undetermined. The interaction between chromophores and the phonons of the surrounding protein matrix make the situation more complicated [6]. To avoid the combined effects of the pigment–pigment and pigment–protein interactions, in vitro aggregates of chromophores in an inert bulk solvent can be prepared. These aggregates serve as suitable models for the investigation of the pure pigment–pigment interactions in the photosynthetic systems.

Growing interest has been devoted to the investigations of dimers and higher oligomers of porphyrins and chlorophylls suited for the modelling of the excitation energy transfer and charge separation in the natural systems [7–10]. The aqueous aggregates of bacteriochlorophyll *c* (BChl *c*) have been used to mimic the intact chlorosomes of the green photosynthetic bacteria. The steady-state spectra (absorption, fluorescence, circular dichroism, linear dichroism) of the model aggregates are very similar to those of the in vivo complexes [11,12]. The water-bound aggregates of chlorophyll *a* (Chl *a*) form cylindrical adducts that also resemble closely the pigment structure of the chlorosomes [13]. The comparable characteristics that have been observed by steady-state and time-resolved spectroscopies have made the investigations of the in vitro Chl *a* water-adducts especially interesting [14,15].

The aggregation of chlorophylls (Chls) mainly arises from the acceptor–donor properties of the Chl macrocycle. The central magnesium atom of a Chl molecule is unsaturated and it has a strong tendency to become occupied by one or two extraneous ligands that act as electron-pair donors. The saturation can also be established by the coordination of other Chl molecules (self-aggregation). The self-aggregation is preferentially caused by the interaction between the central magnesium atom and the oxo group at position C-13^1 [16]. Additional donor groups in Chl *a* are the ester carbonyls of the C-13^2 methoxycarbonyl and the C-17 phytoxycarbonylethyl side-chains (Fig. 1).

In nonpolar solvents Chl *a* self-aggregates, but an addition of strong nucleophiles (pyridine, acetone) results in their immediate coordination to the central magnesium atom, thereby replacing the other Chl *a* molecules that may be bound to it. The result is a monomeric Chl *a* solution [17]. Some molecules are able to link together Chl molecules to yield even very sizable polymeric structures. In aliphatic hydrocarbons, the addition of a slight amount of water to a self-aggregated Chl *a* solution results in the appearance of sizable Chl *a* water-adducts. In these adducts, one electron-pair of the oxygen atom in the water molecule, establishes a bond with the central magnesium atom of a Chl *a* molecule. One hydrogen atom

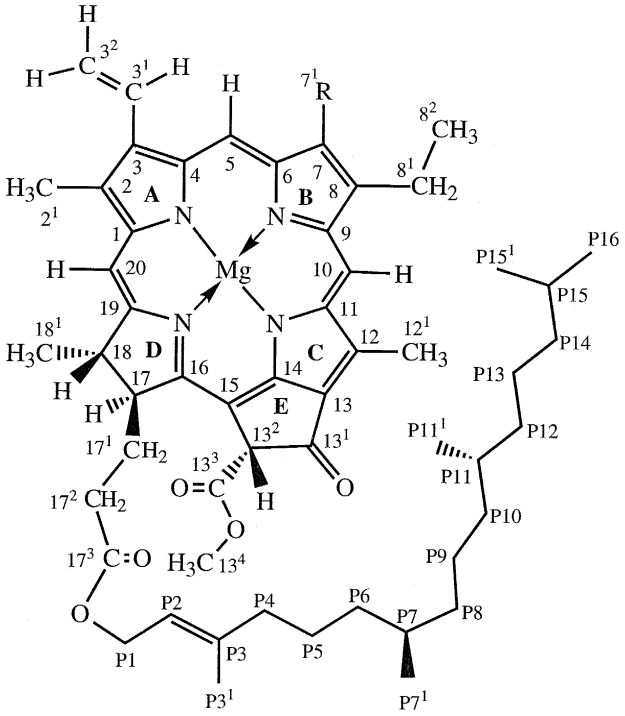

Fig. 1. Structrure and numbering system of Chl *a*, R = CH_3 (methyl).

of the water molecule hydrogen bonds with the C-13[1] oxo group of an adjacent Chl *a* molecule. When a large number of Chl *a* molecules are bound together in the same manner, an ordered aggregate structure is formed [13,14]. Chl *a* and other chlorophylls contain several possible sites for hydrogen bonding with water molecules. Therefore, the structure of the Chl *a* water-adduct and the bonding of water molecules within the adduct frame, have remained to some extent unclear.

Polymeric ordered aggregates of chlorophylls and their derivatives, where the pigments are cross-linked by dioxane, a bifunctional ligand, are particularly suitable for the modelling of pigment–pigment interactions. The two oxygen atoms of the dioxane molecule are able to link two chlorophyll molecules by coordinating to the central magnesium atoms of the chlorophylls. Due to the molecular structure of dioxane, other types of bonding are not possible (compare to the hydrogen bonding in the case of water) and the number of potential aggregate structures is thus effectively diminished. The polymeric aggregates of Chl *a* have previously been studied in a binary mixture of water and dioxane (4:1), and also in a mixture of water and morpholine [18,19]. When concentrated solutions of Chl *a* in castor oil were treated with dioxane vapours, a new absorption band, centred at 687 nm, appeared as a result of aggregation [19]. The aggregation induced a red-shift of 24 nm (527 cm^{-1}) relative to the monomeric Chl *a* (λ_{max} at 663 nm).

In this work, we have prepared dioxane-bound polymeric aggregates of Chl *a* in 3-methylpentane (3-MP). The binary mixture of water and dioxane can cause several problems for the interpretation of spectroscopic data, since also the water molecules easily work as extraneous ligands between the chlorophyll macrocycles. It may be difficult to say to what extent the aggregation is due to dioxane. We used the 3-MP as a solvent, since it generates an inert solvent bulk around the aggregates. To study the aggregates, we have utilized steady-state UV/visible absorption spectroscopy, fluorescence spectroscopy and circular dichroism (CD) both at room temperature and at 77 K. Also the time-resolved emission kinetics was determined at different emission wavelengths and at high and at low temperatures. The aim of this study is to find correlations between the spectral-kinetic characteristics and structural organization induced by the aggregation of Chl *a*.

2. Materials and methods

The preparation of the sample started by dissolving 0.50–1.00 mg of solid Chl *a* in 10 ml of 3-methylpentane (3-MP) (Fluka Chemica, > 99%). The solid, essentially anhydrous Chl *a* was prepared by the large-scale modification (Hynninen, P.H., unpublished data) method of Hynninen [20,21]. The spectroscopic properties (UV/visible absorption, ^1H NMR) of the Chl *a* preparation were consistent with the values published previously [21]. The solvent (3-MP) was carefully dried by passing it through a column filled with activated aluminium oxide; the solvent was stored over 4 Å molecular sieves. Anhydrous Chl *a* was dissolved in dry 3-MP to give a partially self-aggregated sample with a nominal Chl *a* concentration of $1 \cdot 10^{-4}$ M. The electronic absorption spectrum of this sample showed a main peak at 663 nm, arising from monomeric Chl *a*, and a shoulder at 674 nm, representing the self-aggregate [14].

In this study, the cross-linking of Chl *a* molecules was established by dioxane. When 1 μl of dioxane was added to 10 ml of dry-aggregate solution, and the sample was mixed for 10 min, Chl *a* dioxane-aggregates were readily formed. When the Chl *a* concentration was decreased to $2.5 \cdot 10^{-5}$ M, the sample still remained in the dioxane-aggregate form. Further dilution of the sample yielded the dry-aggregate spectrum. Addition of an excess of dioxane induced a rapid aggregation and visible particles appeared in 5 min. This led to the precipitation of the Chl *a*-dioxane-aggregates and after 10 min a sizable precipitate had formed on the bottom of the sample bottle. After some hours, the sample reached a dynamic equilibrium in which the aggregate concentration in the liquid phase remained constant. If the dioxane concentration was within the right range, the sample was stable for several days and no precipitation was observed. The state of the sample could be easily controlled by electronic absorption and fluorescence spectroscopies. We have performed measurements for freshly prepared samples and also for samples that had reached the equilibrium between the solid and the liquid state. The spectral properties of these two

types of samples were found to be essentially the same. To obtain a stable sample, several samples were prepared and the most stable one was selected for further experiments.

The absorption spectra were measured by using a Specord M 40 (Carl Zeiss, Jena, Germany) UV/vis Spectrophotometer. The steady-state emission and excitation spectra, corrected for spectral sensitivity distribution of the excitation light, were scanned with a hand-made laboratory set-up [22]. The system was used at 77 K and at 293 K. The polarized fluorescence spectra were recorded with the same spectrometer. The system was based on two grating monochromators (MDR-23). A high pressure Xenon lamp (DKSSH-3000) with a water cooling system was used for excitation. The fluorescence from the sample was modulated by a disk modulator and the emission light was directed to a recording monochromator. A photomultiplier (FEU-83) with an additional cooling system was used for the emission detection. Two Glan prizms (a polarizer after the exciting monochromator and an analyzer before the recording monochromator) were used for the polarized fluorescence measurements. The angle between the polarized excitation beam and the registration direction was 90°. The polarization degree (P) was calculated from Eq. (1):

$$P = \frac{I_V - kI_H}{I_V + kI_H} \quad (1)$$

where I_V and I_H are the vertical and the horizontal components of the fluorescence intensity, respectively. The experimental factor (k) depends on the registration wavelength and is determined by the difference between the sensitivity of the recording channel to the vertically and horizontally polarized light.

The circular dichroism (CD) spectra were measured on a JASCO Model 20 spectropolarimeter. At 293 K, 2–10 mm pathlength quartz cuvettes were used. The 77 K spectra were recorded after a quick cooling of the sample in order to avoid precipitation of the sample on the walls of the cuvette. A special rectangular cryostat was used at liquid nitrogen temperatures. Glass cuvettes with a pathlength of 1–2 mm were found more suitable than the quarz cuvettes for low-temperature measurements, to avoid the precipitation of the sample on the walls of the cuvette.

The single-photon-counting (SPC) experiments were based on a Coherent MIRA 900 Ti:sapphire laser. The excitation pulse width was 200 fs. The repetition rate of the laser is originally 76 MHz but it was decreased to 5 MHz with a pulse picker. A non-linear crystal ($LiIO_3$) was used for the frequency-doubling of the excitation beam. After the crystal, a harmonic separator was placed to split the fundamental and second harmonic light. The fundamental light was reflected to a diode, which generated the stop-pulse of the system. The second harmonic light was used for the excitation of the sample and the fluorescence was collimated with a lens at right angle with respect to the excitation light. The fluorescence light was passed through a polarizer. A 10 nm band-pass interference filter selected the required emission wavelength. Finally, the fluorescence light was directed on a multichannel plate (MCP). The intensity of the excitation light was set to a level which produces approximately one fluorescence photon on the MCP from every 100 excitation pulses. A typical excitation light intensity used was $1 \cdot 10^{11}$ photons $\text{pulse}^{-1} \cdot \text{cm}^{-2}$. A linear amplifier generated the start-pulse after the MCP. The pulses from the MCP and from the stop-diode were both passed through comparators. A time-to-pulse-height converter (Ortec) produced a pulse, whose amplitude was dependent on the time-delay between the start- and stop-pulses. The pulses were acquired on corresponding time-delay channels in the multichannel pulse-height analyzer (Nokia Electronics LP 4700). The counts were recorded during a constant time. A minimum of 10,000 counts were required for the maximum channel in order to accept the data for further processing. The data was transported to a computer, which displayed the decay trace in the time domain. The instrument function of the system was 50 ps. The data was convoluted with a commercial Globals Unlimited software program.

3. Results

The interpretation of the absorption spectrum of the Chl *a* dioxane-aggregate in 3-MP is not straightforward. When Chl *a* forms aggregates in water-dioxane mixtures (4:1), a single Q_y band is established at 687 nm. In spite of the simplifying solvent selec-

tion in this study, the Q_y-region of the absorption spectrum of the Chl *a* dioxane-aggregate is more complicated in 3-MP preparations than in the case of water-dioxane mixtures (Fig. 2).

At 77 K, the Q_y-region in the absorption spectrum of the Chl *a* dioxane-aggregate shows four clearly resolvable bands. A deconvolution into six Gaussian components is required to obtain a good fit for the long-wavelength side of the low-temperature spectrum. The central wavelengths and the full-widths at the half-maxima (FWHM) of the bands are given in Table 1. The blue-most band of the four major bands lies at 683 nm. The FWHM of the 683 nm band is 95 cm^{-1}. In order to be able to fit the blue side of the 683 nm band, which shows considerable tailing, a Gaussian component centred at 678 nm is needed. The second major band appears at 689 nm, and the width of the band is approximately the same as that of the 683 nm band. Also the intensities are comparable. The two longest-wavelength bands possess peaks at 698 nm and at 702 nm. The corresponding Gaussian components are extraordinarily narrow with FWHM-values of 64 cm^{-1} and 43 cm^{-1}, respectively. The experimental longest-wavelength band tails slightly to the red and, hence, a sixth Gaussian component, centred at 704 nm, is needed for a proper fitting of the absorption spectrum. The room-temperature absorption spectrum does not differ significantly from the low-temperature spectrum, except for the number of Gaussian bands required in the fitting process. A five-component fit is adequate, since the longest-wavelength band is absent or has a very low intensity at room-temperature. The resolution of the 293 K spectrum is diminished due to the broadening of the bands. Some minor shifts of band maxima are also observed. At low temperature, the fractional intensities of the main four bands are particularly close to one another, whereas at 293 K, the band intensities show noticeable differences.

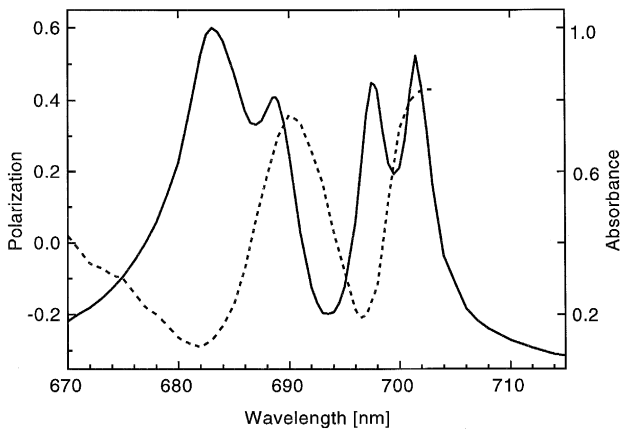

Fig. 2. Q_y region of the low-temperature absorption spectrum of the Chl *a*-dioxane aggregate (————), and the corresponding fluorescence polarization spectrum (---), measured at 77 K. Emission was detected at 702 nm.

Table 1
Spectral values characteristic of the six Gaussian bands used in the deconvolution of the absorption spectrum of the Chl *a*-dioxane aggregate at 77 K

λ_{max} (nm)	Full-width at the half maximum of the band (cm^{-1})	Relative integrated intensity of the band
678	216	0.20
683	95	0.24
689	92	0.21
698	64	0.17
702	43	0.11
704	99	0.07

The polarization spectrum of the Chl *a*-dioxane aggregate was measured at liquid nitrogen and at room-temperatures. A plot of the fluorescence polarization versus excitation wavelength was achieved for the Q_y and Soret regions. The polarization of the emission was detected at 702 nm and the values of polarization were transformed into steady-state anisotropy digits using Eq. (2):

$$r = \frac{2P}{3 - P} \tag{2}$$

where r denotes the steady-state anisotropy and P is the degree of polarization. In a vitrified and dilute solution the polarization spectrum provides a measure of the angle between the absorption and the emission transition dipoles of the molecules [23]. In our case, the 3-MP solvent forms a glass at 77 K, in which the aggregates remain immobile during the lifetime of the excited state. Also the chromophore concentration ($1 \cdot 10^{-4}$ mol/l) is low enough to prevent a noticeable dynamic energy transfer between the individual aggregate units. The angle (θ) between the absorp-

tion and the emission transition dipoles was calculated from Eq. (3):

$$\theta = \arccos^2 \frac{5r + 1}{3} \quad (3)$$

The values of polarization, anisotropy and the angle θ at certain wavelengths are listed in Table 2. The theoretical limits for the values of polarization are $0.33 \leq P \leq 0.5$ in an isotropic solution.

The low-temperature absorption spectrum with well-resolved transitions, shows a high-resolution polarization spectrum (Fig. 2). The degree of polarization varies markedly within the Q_y-band region. The absorption spectrum contains four clearly resolvable bands. The longest-wavelength band, centred at 702 nm, has the highest degree of polarization (0.43). Eqs. (2) and (3) yield the angle between the absorption and the emission transition moments to be 19° for this red-most transition. On going to 697 nm, the polarization drops all the way down to -0.21. At 690 nm, the polarization is again positive with a value of 0.36. The blue-most band has the minimum *P*-value of -0.29 at 682 nm, and the corresponding θ-value is 79°. The polarization spectrum of the Soret-region (not shown) peaks at 451 nm with a maximum *P*-value of 0.18. In the region from 440 to 380 nm, the polarization spectrum experiences only minor changes and the polarization values are in the range $-0.13 \leq P \leq -0.02$. The principal structure of the room-temperature polarization spectrum does not differ from the low-temperature spectrum. The broadening of the bands, resulting in overlapping between the absorptions, causes the polarization to change smoothly as a function of wavelength. The overlapping also ensures that as high values of polarization as those at 77 K are not recorded.

Table 2
Values of polarization (P) for the polarization spectrum of the Chl *a*-dioxane aggregate at 77 K, and the corresponding values of anisotropy (r) and the angles (θ) between the absorption and emission transition moments

λ (nm)	P	r	θ
451	0.18	0.13	42
682	−0.29	−0.18	79
690	0.36	0.27	27
697	−0.21	−0.13	70
702	0.43	0.34	19

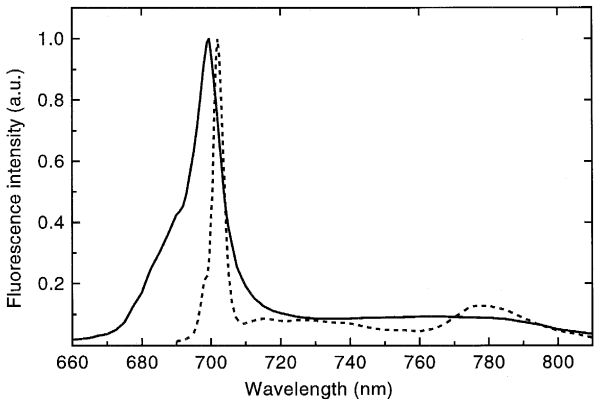

Fig. 3. Emission spectra of the Chl *a*-dioxane aggregate at 293 K (————) and at 77 K (---). Wavelengths of excitation were 446 nm (293 K) and 442 nm (77 K). The spectra were normalized to unity.

The emission spectra of the aggregate region were recorded at high and at low temperatures (Fig. 3). The excitation wavelengths were 446 nm (293 K) and 442 nm (77 K). At room-temperature, the fit of the emission spectrum with three Gaussian components, suggests the presence of two distinct, clearly resolved bands and a long tail on the red side of the spectrum. The blue-side emission maximum peaks at 695 nm and the FWHM of the band is 416 cm^{-1}. The second emission band, centred at 699 nm, is markedly narrower with an FWHM of 112 cm^{-1}. The integrated intensity of the 695 nm band is 3-fold that of the 699 nm band. The room-temperature emission spectrum spans to the red all the way upto 800 nm. At 77 K the red-side emission band becomes very narrow (FWHM = 59 cm^{-1}) and its maximum is shifted to 702 nm. The intensity of the second band decreases and the maximum of the band lies at 699 nm (FWHM = 73 cm^{-1}). Also the low-temperature emission spectrum tails to the red. When the emission spectrum is measured at 77 K, one striking difference becomes evident. At the wavelength region of 770–790 nm, a completely new and a rather broad emission band appears. The integrated intensity of this red-most emission band is approximately the same as that of the 702 nm emission band.

The high and low-temperature CD spectra were measured in the 350–730-nm range. In the Soret-region (spectrum not shown), the CD amplitude is low experiencing only minor changes around zero, until a

substantially strong positive band, centred at 443 nm, becomes apparent at room-temperature. On lowering the temperature to 77 K, this band moves to 446 nm. At 293 K, the CD-curve crosses the zero-level at 449 nm and turns into negative again. A symmetric and negative band with high intensity, and an FWHM of 480 cm^{-1} is centred at 456 nm. The low-temperature CD spectrum in the Soret-region becomes negative at 446 nm, resulting in a negative band centred at 454 nm. The low-temperature band is somewhat broader (FWHM = 580 cm^{-1}) than the high-temperature band. Both the 77 K and the 293 K CD spectra remain slightly negative until they reach the Q_y-region of the spectrum.

The Q_y-region of the low-temperature CD spectrum was deconvoluted into five Gaussian components (Fig. 4). On the high-energy side, the CD-signal is weak and negative until at 675 nm it turns into positive. The fit suggests the presence of two positive bands, centred at 685 and 691 nm. The spectral parameters of the CD-spectra are listed in Table 3. At 694 nm, the CD-curve crosses the zero-line and then turns into negative. The rest of the CD-spectrum consists of two negative bands and of a small positive contribution at 702 nm. For a proper fitting of the CD spectrum after 694 nm, three bands, centred at 696 nm (−), 702 nm (+) and 704 nm (−) are needed. The red-most band at 704 nm is noticeably broader and more intense that the two others. The room-temperature CD spectrum is also fitted best with five Gaussian bands. Some changes are observed, when the CD spectra measured at two different temperatures are compared. The first band on the blue side of

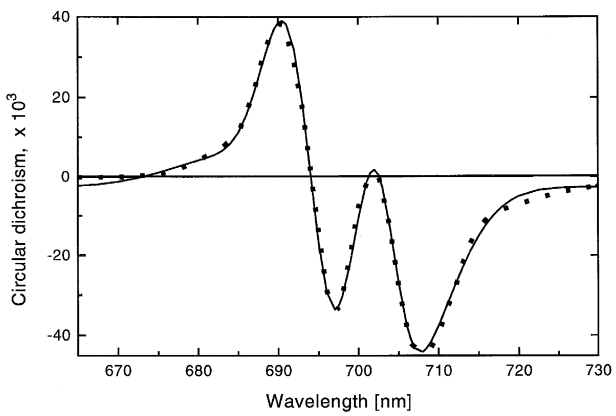

Fig. 4. CD spectrum of the Chl *a*-dioxane aggregate at 77 K (■ ■ ■ ■) and a fit with five Gaussian bands (————).

Table 3
Spectral values characteristic of the five Gaussian bands used in the deconvolution of the CD spectrum of the Chl *a*-dioxane aggregate at 77 K and at 293 K

Temperature (K)	λ_{max} (nm) and sign	Full-width at the half maximum (cm^{-1})	Negative area/total area
293	682 (−)	186	0.52
293	691 (+)	133	
293	698 (−)	145	
293	699 (+)	72	
293	705 (−)	145	
77	685 (+)	339	0.68
77	691 (+)	132	
77	696 (−)	85	
77	702 (+)	97	
77	704 (−)	250	

the 293 K spectrum is negative and centred at 682 nm, whereas at 77 K, this band is positive and lies at 685 nm. The relative intensities of the two bands at 691 nm (positive) and at 698 nm (negative) in the room-temperature spectrum are substantially higher than those of the corresponding bands in the low-temperature spectrum. In addition, the intensity and the width of the red-most band in the room-temperature spectrum are considerably lower than in the case of the 77 K spectrum.

The time-resolved decays of fluorescence were measured both at 293 K and at 77 K at different wavelengths of emission (Fig. 5). The excitation light wavelength was 460 nm for both temperatures. The decay traces were recorded for three directions of polarization. The components of emitted light, polarized parallel ($I_{\|}(t)$) and perpendicular ($I_{\perp}(t)$) to the electric vector of the exciting light, were measured. The magic angle (an angle of 54.7° between the excitation and the emission polarizers) conditions gave the polarization independent, isotropic fluorescence decay. The time-resolved decay of fluorescence anisotropy was calculated for most emission wavelengths. The anisotropy decay was obtained from the parallel and perpendicular sets of measurements according to Eq. (4):

$$r(t) = \frac{I_{\|}(t) - I_{\perp}(t)}{I_{\|}(t) + 2I_{\perp}(t)} \quad (4)$$

The anisotropy decay function was fitted with a single exponential.

A three-component global-analysis fitting procedure was applied to the complete set of kinetic traces measured at 77 K at various emission wavelengths. The emission decays for individual wavelengths were also deconvoluted separately. The kinetic constants of the isotropic decays and the information from the anisotropy measurements are listed in Table 4. The room-temperature kinetics were fitted best with a global analysis consisting of two decay components. There is one obvious difference between the low-temperature and the high-temperature kinetics. In the low-temperature decays, when the red-most emissions are detected, a clear lifetime component in the nanosecond range becomes evident. In the room-temperature kinetics, such a component does not exist. A three-component global analysis for the 77 K emissions gives the lifetimes of 95 ps, 1.1 ns and 5.2 ns. When the decay traces were deconvoluted separately, 1–3 decay components were used. The criteria for the selection of the amount of components were the quality and the simplicity of the fit. The deconvolution was carried out with as few components as possible to get a reasonable fit to the data.

The low-temperature emission detected at 656 nm has a single component with a lifetime of 6.1 ns. The 675 nm emission is best fitted with a double exponential possessing components of 130 ps and 6.7 ns with almost equal amplitudes. The decay of the fluo-

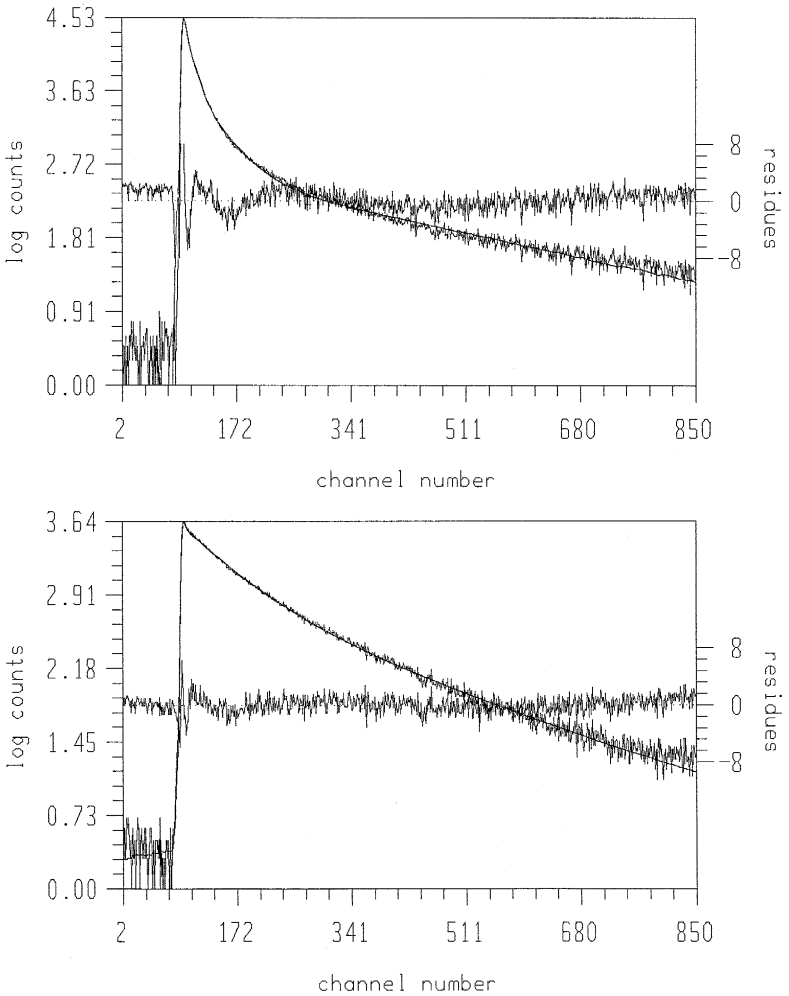

Fig. 5. Emission kinetics of the Chl *a*-dioxane aggregate at 77 K. Excitation wavelength was 460 nm and the emission was collected at 713 nm (upper curve) and at 753 nm (lower curve). The plots show the decays and the fits. Also plotted are the residuals. The time window is 11 ns. The device function of the single-photon counting system was 50 ps.

Table 4
Kinetic parameters characteristic of the Chl *a*-dioxane aggregate sample at 77 K and at 293 K

Temperature (K)	$\lambda_{emission}$ (nm)	τ_1 (ps)	α_1	τ_2	α_2	τ_3 (ns)	α_3	$\tau_{anisotr.}$	r_0	r_∞	χ^2
77	656					6.1	1.00				1.31
77	675	130	0.60			6.7	0.40	90 ps	0.18	0.14	1.13
77	702	40	0.92	210 ps	0.07	4.4	0.01	2.2 ns	0.26	0.21	8.03
77	713	90	0.91	500 ps	0.08	3.8	0.01	no decay	0.01	0.01	10.1
77	736	220	0.46	1.1 ns	0.48	3.4	0.06	no decay	0.04	0.02	1.76
77	753	100	0.49	1.0 ns	0.43	2.9	0.08				1.43
77	787	300	0.45	1.7 ns	0.55						1.27
293	656					5.3	1.00				1.04
293	675	90	0.63			5.1	0.37	no decay	0.03	0.03	1.23
293	702	60	0.86	210 ps	0.13	4.5	0.01	550 ps	0.14	0.04	1.50
293	713	70	0.88	220 ps	0.11	4.5	0.01	600 ps	0.14	0.07	1.27
293	736	70	0.92	350 ps	0.05	4.7	0.03	510 ps	0.15	0.01	1.13
Three-comp. global analysis at 77 K		95		1.1 ns		5.2					
Two-comp. global analysis at 293 K		110				5.4					

rescence anisotropy is very small and therefore not well resolved. The initial anisotropy is 0.18 and it drops down to 0.14 with a lifetime around 100 ps. The fitting of the 702 nm and 713 nm emissions is very difficult, since the decays are highly multiexponential. The goodness of the fit is described by the value of χ^2, and for these two emission wavelengths the χ^2 value is almost 10-fold the value for the rest of the separately deconvoluted decays in this study. This indicates that at these wavelengths the decay is not described accurately with a sum of three exponential functions or any exponential functions. However, we used a three-exponential fit also for these time-resolved emissions in order to keep the interpretation of the data as straightforward as possible. A fit with three components suggests the precence of a short lifetime below 100 ps. The fractional intensity of this first component is very high. The second component is several hundreds of picoseconds long with an amplitude one-tenth of that of the shortest component. The long-lived component is several ns. One major difference exists between the 702 and 713 nm emission wavelengths. The initial fluorescence anisotropy of the 702 nm emission is 0.26 and it decays clearly to a value of 0.21 within a time constant of 2.2 ns. In contrast, no decay of fluorescence anisotropy can be resolved for the 713 nm emission. The fluorescence anisotropy function is just a constant value of 0.01 even at the very beginning of the emission.

The wavelength range of 736–787 nm produces again good fits. The excistence of a component with a lifetime of approximately 100–300 ps is seen for all long-wavelength emissions. An intermediate component with a lifetime of 1.0–1.7 ns becomes evident with a comparable amplitude. Also a third component with a lifetime of a few ns is present with a rather low amplitude. At 787 nm, the emission lacks the longest lifetime and is best fitted with a double-exponential. The fluorescence anisotropy of the 736 nm emission remains at the zero-level. For the 753 nm and 787 nm emissions, only isotropic kinetics were measured.

The room-temperature emissions were collected at five emission wavelengths. A three-component global analysis gives the lifetimes of 70 ps, 260 ps and 5.1 ns. However, an equally good fit is obtained with a global analysis of only two components, which gives the lifetimes of 110 ps and 5.4 ns. The component, which is around 1–2 ns at 77 K, obviously cannot be found by the room-temperature measurements. When the decay traces are deconvoluted individually, the first emission at 656 nm is best fitted with a single exponential having a lifetime of 5.3 ns. The fit at 675 nm suggests the appearance of two components having comparable amplitudes and lifetimes of 90 ps and 5.1 ns. The three last emission decay profiles produce best fits with three exponentials. All three emissions have a short component around 60–70 ps. The intermediate lifetime is within the range of 200–350 ps.

The long-lived component around 4.5 ns can be found for all these traces. For the 675 nm emission, no decay of fluorescence anisotropy can be resolved. The anisotropy is very low for all times, having a value of 0.03. In the range from 702 nm to 736 nm, the emissions exhibit a decaying fluorescence anisotropy with a lifetime of 500–600 ps. The initial anisotropy for these emissions is 0.14 and the residual anisotropy remains at the level of 0.01–0.07.

4. Discussion

Concerning the dioxane-bound aggregates of Chl *a* in 3-MP, the main questions involve the amounts of different species present in solution, the structures of the species and the extent of their mutual interaction. It is clear that spectrally different types are formed in 3-MP. We propose that the diverse spectral forms arise from different arrangements of the interacting Q_y-dipoles, or different Chl *a*-Chl *a* intercentre distances within the aggregate. In the dipole–dipole approximation, the interaction energy and corresponding splitting depends on the distance between the dipoles and on their mutual orientation [24]. In addition, the dissimilar spectroscopic characteristics can arise from the differences in the number of molecules in the aggregates. The precipitation of the sample indicates that large aggregate structures are formed and that also the long-range interactions within the aggregates are possible.

The absorption spectrum of the Chl *a*-dioxane-aggregate (Fig. 2) shows four principal absorption bands in the Q_y region both at room and liquid nitrogen temperatures, suggesting the presence of more than one type of aggregate. At 77 K, the four separate Q_y-bands have comparable intensities and bandwidths. The deconvolution of the 77 K absorption spectrum of the dioxane-bound Chl *a* aggregate gives six bands. The band at 678 nm is markedly broader than the other bands indicating strong inhomogeneity inside it. The Chl *a* self-aggregates of various sizes in 3-MP induce a broad and inhomogeneous absorption band, which has the maximum at 674 nm [14,25]. We believe that the 678 nm absorption band arises from a mixture of Chl *a* self-aggregates and dioxane-bound aggregates possessing a low aggregation number. Highly expected is that also dioxane molecules are partially mixed in to the self-aggregates of Chl *a*. The low CD-intensity within this region verifies that large and ordered aggregate structures are not present.

In the preparations of Chl *a*-dioxane aggregate in an aliphatic hydrocarbon, the presence of residual monomeric Chl *a* cannot be avoided. Owing to their high fluorescence quantum yield, the residual monomers usually hinder the detection of the aggregate fluorescence. In the excitation spectrum of Chl *a*-dioxane aggregates only a minute contribution from monomer fluorescence at the excitation wavelength around 450 nm is seen (Fig. 6). When the emission is detected at 705 nm, it has the strongest contribution from the aggregates and the excitation spectrum shows a strong maximum at 450 nm. Even though the sample is excited at 442–446 nm, some contribution to the fluorescence from the Chl *a* monomers and small aggregates is expected. In the room-temperature SPC measurements at 656 nm, a single lifetime-component of 5.3 ns corresponds to the value of 5.1 ns previously observed for the fluorescence lifetime of monomeric Chl *a* in 3-MP at room-temperature [16]. The emission kinetics at the registration wavelength of 675 nm begin to show a contribution from a short-lived component, verifying the presence of the aggregate emission already at this emission wavelength. The room-temperature kinetics show no decay of anisotropy at 675 nm, and the anisotropy level remains at 0.03 for longer times also. This result is in

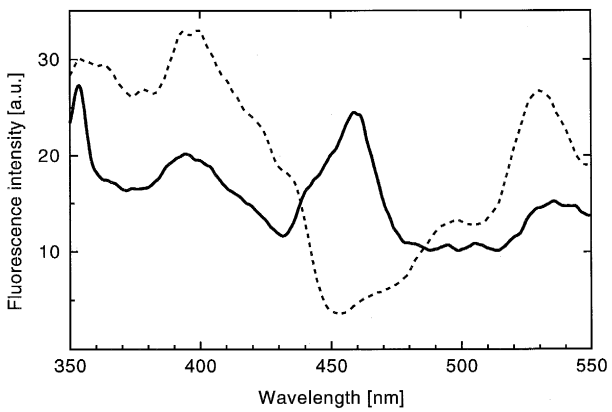

Fig. 6. Soret region of the excitation spectrum of the Chl *a*-dioxane aggregate when the emission was detected at 663 nm (---) and at 705 nm (————).

agreement with the fluorescence anisotropy measurements of monomeric Chl *a* in castor oil [26].

The fluorescence of the Chl *a*-dioxane aggregates is surprisingly high. Usually the aggregation of the pigments decreases the fluorescence quantum yield rapidly as a function of the aggregation number. Superradiant fluorescence has previously been detected from the aggregates of pseudoisocyanine bromide (PIC-Br) [27–29]. One common feature of this type of aggregates is a very sharp and red-shifted absorption line, referred to as a J-band. In J-aggregates, the orientations of the Q_y transition dipoles are roughly in the same plane in a head-to-tail fashion. The absorption and fluorescence spectra of the Chl *a*-dioxane aggregates show characteristics similar to those of the PIC-Br aggregates. The absorption and emission bands are very narrow already at 77 K. In order to show features common to those of J-aggregates, sizable aggregate structures have to be present in the Chl *a*-dioxane aggregate sample. This is supported by a simple visual observation: the sample is unstable and tends to precipitate indicating the appearance of large macromolecular particles.

The excitation spectrum of the Chl *a*-dioxane aggregate is virtually identical with the absorption spectrum, when the emission is detected in the wavelength range of 700–780 nm. The same four major bands that are observed in the absorption spectrum are also present in the excitation spectrum. An attractive way to interpretate the data is that there are two spectrally different forms of excitonically strongly coupled pigments present in the same aggregate frame. The existence of two species is supported by the observation of two strong emission bands. The low Chl *a* concentration in our samples should maintain the level of dynamic energy transfer between separate particles so low that the observed spectroscopic properties could only be explained by the existence of one aggregate species. The basic spectroscopic unit could be a strongly bound dimer, which is supposed to be the elementary subunit in many photosynthetic antenna systems [30]. Also a small dioxane-bound oligomer could function as an elementary subunit. The difference in energy could be induced by the differences in the numbers of interacting pigments or by the dissimilar orientations or distances between the Q_y transition dipoles of the chromophores. With a certain orientation of the interacting Q_y-dipoles, the splitting into two excitonic bands with comparable intensities is observed [31]. The absorption spectrum of the Chl *a*-dioxane aggregate shows four sharp transitions with comparable intensities and an abrupt change in polarization between the absorption bands. The transition dipoles of the two excitonic states in an excitonically coupled dimer are perpendicular to each other. The four absorption bands in the Q_y-region with high positive and negative polarization values could be explained to arise from two types of elementary units that show high- and low-energy excitonic transitions. It is important to note that the fluorescence polarization spectrum has positive and negative *P*-values which approach the theoretical limits. If effective energy transfer in the aggregate is assumed, the high degree of polarization may be detected for highly ordered structures only.

The two main emission bands at 702 and 699 nm are very narrow at 77 K (Fig. 7). The supposition that the 702 nm absorption band is responsible of the stronger emission band at 702 nm is supported by the absence of Stoke's shift between the absorption and emission λ_{max}-values which is in common to the J-aggregates. If it is assumed, in addition, that the 702 nm absorption band represents a J-like transition, then the higher-energy excitonic component of the transition could be either the 683 nm or the 698 nm absorption band. The reason for this is the *P*-value, which has to have a sign, opposite to the sign of the 702 nm absorption band in an excitonic system. The small Stoke's shift between the 699 nm emission

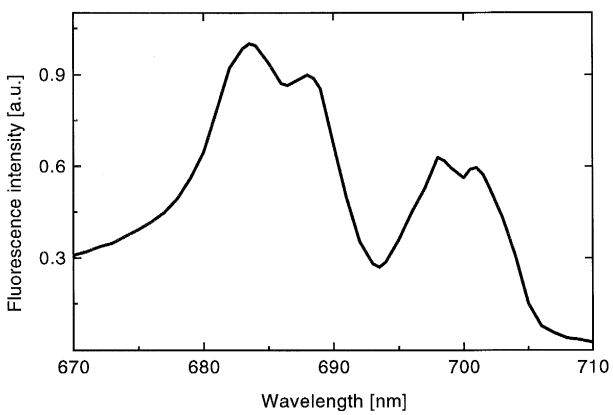

Fig. 7. Q_y region of the excitation spectrum of the Chl *a*-dioxane aggregate at 77 K. The emission was detected at 780 nm.

band and the 698 nm absorption band suggests that the former originates in the latter. Because the 698 nm absorption band is coupled to the 699 nm emission band, it cannot be the higher excitonic band of the 702 nm transition. Following this line of argumentation, the 683 nm and the 702 nm absorptions form the excitonically split spectrum of type I and the 689 nm and the 698 nm absorptions the excitonically split spectrum of type II. The polarization spectrum with highly negative and positive *P*-values for the transition pairs supports this conclusion.

The optical activity of the Chl *a*-dioxane aggregate is high. The CD signal is stronger by more than two orders of magnitude compared to the value found for monomeric Chl *a* in dioxane. The strong CD signal is connected with the excitonic coupling of the resonant and strong Q_y-transitions of the molecular subunits in the aggregate. In the Q_y-band region of the 293 K absorption spectrum, the splitting into components of opposite signs is observed. At 293 K, the sequence of splitted components and their signs reflect the situation observed in the polarization spectrum. The integrated area under the negative and positive CD bands is practically the same, also manifesting the excitonic nature of the 293 K CD spectrum. The signs of the CD bands support the existence of type I and type II spectral forms.

Upon lowering the temperature to 77 K, the intensity of the CD signal is enhanced and also the conservative nature of the spectrum disappears. The CD band at 685 nm becomes very broad and positive in sign in the low-temperature spectrum. We propose that differential light-scattering takes place and that a ψ-type circular dichroism is observed. The ψ-type circular dichroism has been previously observed for large biological macroaggregates such as DNA-aggregates and chlorophyll *a*/*b* light-harvesting antenna complexes [32,33]. One requirement for a ψ-type CD signal is the size of the aggregate, which has to be at least $1/4$ of the wavelength of the light interacting with the aggregate. In addition, the aggregate must have a high density of interacting dipoles, leading to some extent delocalized light-induced excitation. Also a long-range chiral structure is required to produce a ψ-type CD signal. The Chl *a*-dioxane aggregates are precipitated from the sample indicating that the aggregates are of macroscopic size. Our tentative molecular modelling results show (Linnanto, J., Oksanen, J.A.I., Helenius, V.M., Peltola, T. and Korppi-Tommola, J.E.I., unpublished data) that the Chl *a*-dioxane aggregate tends to curl slightly along the long axis of the aggregate producing a helical structure. The existence of the delocalized excitation is indicated by the short lifetime observed for fluorescence emission.

The low-temperature CD spectrum is clearly affected by long-range interactions giving rise to a ψ-type signal. It is well known that long-range interactions can considerably change some parts of the CD spectrum while other parts remain unchanged. Changes in intensity and sign are often discovered. In the Chl *a*-dioxane sample at 77 K, the band at 685 nm changes its sign from negative to positive. Typically, the presence of a ψ-type contribution is seen when the CD signal appears outside the absorption bands. In our case, the differential light scattering induces a strongly ψ-type CD band to the red-side of the spectrum, even at wavelengths where no absorption is observed. The lowering of the temperature tends to enhance the ψ-type character of the CD signal. For the Chl *a*-dioxane aggregate this behaviour can be observed as a strong increase in the amplitude of the 705 nm CD band. At 730 nm, the low-temperature CD signal has not yet reached the zero-line, even though the absorption has vanished.

Even if the CD-signal is interfered by the ψ-type effects, the excitation delocalization length in the Chl *a*-dioxane aggregates is not analogous to that in the PIC-Br-aggregates. In the PIC-Br-aggregates, the delocalization length extends over a large number of molecules and it is dependent on the temperature due to the thermal phonons that cause intermolecular dephasing. Upon lowering the temperature, the number of coherently coupled molecules increases, the excitation delocalizes over a larger ensemble of molecules and the fluorescence lifetime decreases. In our SPC measurements, we cannot find any major effect of temperature on the emission lifetimes. This can be explained in terms of an excitation, which is delocalized inside an elementary cell of size not more than some molecules. Nevertheless, the non-radiative singlet–singlet energy transfer can take place and the excitation can move from one elementary cell to another, which is demonstrated by the absence of fluorescence anisotropy in the SPC measurements and the independence of the fluorescence excitation

spectra on the recording wavelength. Some changes observed in the emission lifetimes and amplitudes upon raising the temperature, may reflect the increase in the efficiency of the thermally activated backward energy transfer from the long-wavelength aggregate to the short-wavelength one in a coupled complex. The energy separation between the S_1-levels of the type I and type II species is only 82 cm^{-1} and at 293 K, $kT = 205$ cm^{-1}.

Although the CD spectrum is affected by the long-range interactions, the ψ-type character of the spectrum is not very strong. Stronger ψ-type CD-signals have been reported by several authors [14,34,35]. Therefore, the assumption of a short delocalization length and moderate long-range interactions in the Chl *a*-dioxane aggregate is reasonable. On the other hand, the observed energy transfer indicates that excitation moves along the aggregate and that the aggregate sub-units are coupled together. We infer that the behaviour of the Chl *a*-dioxane aggregate lies somewhere between the two extremes of localized and delocalized excitations.

The appearance of the new and broad emission band around 780 nm at liquid nitrogen temperature is an interesting phenomenom. We do not want to emphasize too much the origin of this emission band, since we have not scanned the low-temperature absorption spectrum for the longer wavelengths due to the low sensitivity of the absorption spectrometer in the infrared. It is noteworthy, however, that as the fluorescence is detected at 780 nm, the excitation spectrum shows the same four absorption bands that are present in all excitation spectra. It proves, that this emission is also coupled to the species of both types. At 77 K, where the band was discovered, the kinetics have a lifetime component of around 1–2 ns with a high amplitude. The 1–2 ns lifetime suggests that the emission arises from a very small aggregate, probably a dimer. One interesting interpretation could be the formation of a charge-transfer or an excited-state complex. The very broad and strongly red-shifted emission bands are typical for molecular complexes that are stable only in the excited state. The low temperatures favour the formation of excited-state complexes. The red-shifted fluorescence band could also represent a well-resolved vibrational component of the main emission transition.

5. Conclusions

The spectral properties of the Chl *a*-dioxane aggregate can be explained by the existence of only one type of macroaggregate that has a size of probably several hundreds of nanometers. The precipitation of the aggregate and the observed ψ-type CD signal indicate that the aggregate has a large size. The existence of two fluorescence bands is a proof of the presence of two different fluorescent species. The independence of the excitation spectrum of the emission wavelength and the rapid loss of time-resolved emission anisotropy at certain wavelengths in SPC measurements suggest that the two spectral forms are coupled together by energy transfer in the same macroaggregate frame. The low concentration of Chl *a* in our sample preparations supports the view that the dynamic energy transfer between individual aggregate units in solution is inadequate to explain the characteristics observed for the Chl *a*-dioxane aggregate. The absence of the temperature effect on the fluorescence lifetimes indicates the excitation delocalization length to be small. The absorption spectrum of the aggregate exhibits four narrow absorption bands with comparable intensities. The polarization and the CD spectra indicate that the 683 and 702 nm absorption bands represent the high-and low-energy splitted excitonic transitions of the type l spectral unit. The 689 and 698 nm absorption bands form the second excitonic transition pair belonging to a spectral unit referred as type Il.

Acknowledgements

Financial support under the EU SCIENCE contract No. ERBSC1* CT920796 is gratefully acknowledged. This work was supported in part by the European Science Foundation scientific programme in ‘Biophysics of Photosynthesis.’

References

[1] R. van Grondelle, J.P. Dekker, T. Gillbro, V. Sundström, Biochim. Biophys. Acta 1187 (1994) 1–65.
[2] S. Savikhin, V. Zhu, S. Lin, R.E. Blankenship, W.S. Struve, J. Phys. Chem. 98 (1994) 10322–10334.

[3] T. Bittner, G.P. Wiederrecht, K.-D. Irrgang, G. Renger, M.R. Wasielewski, Chem. Phys. 194 (1995) 311–322.
[4] L.-O. Pålsson, S.E. Tjus, B. Andersson, T. Gillbro, Chem. Phys. 194 (1995) 291–302.
[5] S.E. Bradforth, R. Jimenez, F. van Mourik, R. van Grondelle, G.R. Fleming, J. Phys. Chem. 99 (1995) 16179–16191.
[6] T. Pullerits, R. Monshouwer, F. van Mourik, R. van Grondelle, Chem. Phys. 194 (1995) 395–407.
[7] M.R. Wasielewski, Chem. Rev. 92 (1992) 435–461.
[8] J.I. Sessler, B. Wang, A. Harriman, J. Am. Chem. Soc. 117 (1995) 704.
[9] A.V. Chernook, A.M. Shulga, E.I. Zenkevich, U. Rempel, C. von Borczyskowski, J. Phys. Chem. 100 (1996) 1918–1926.
[10] V.S. Chirvonyi, E.I. Zenkevich, R. Gadonas, V. Krasauskas, A. Pelakauskas, in: Laser Applications in Life Sciences, SPIE, vol. 1403, part I, 1991, pp. 638–639.
[11] M. Miller, T. Gillbro, J.M. Olson, Photochem. Photobiol. 57 (1993) 98–102.
[12] M. Hirota, T. Moriyama, K. Shimada, M. Miller, J.M. Olson, K. Matsuura, Biochim. Biophys. Acta 1099 (1992) 271–274.
[13] J.J. Katz, M.K. Bowman, T.J. Michalski, D.L. Worcester, in: H. Scheer (Ed.), Chlorophylls, CRC Press, Boca Raton, FL, 1991, pp. 211–236.
[14] J.A.I. Oksanen, V.M. Helenius, P.H. Hynninen, H. van Amerongen, J.E.I. Korppi-Tommola, R. van Grondelle, Photochem. Photobiol. 64 (1996) 356–362.
[15] V.M. Helenius, J.O. Siikki, P.H. Hynninen, J.E.I. Korppi-Tommola, Chem. Phys. Lett. 226 (1994) 137–143.
[16] V.M. Helenius, P.H. Hynninen, J.E.I. Korppi-Tommola, Photochem. Photobiol. 58 (1993) 867–873.
[17] J.J. Katz, L.L. Shipman, T.M. Cotton and T.R. Janson, in: D. Dolphin (Ed.), The Porphyrins: Physical Chemistry, Part C, vol. V, Academic Press, New York, 1978, pp. 401–458.
[18] E.I. Zenkevich, M.V. Sarzhevskaya, T.V. Vitovtzeva, J. Appl. Spectr., 37 (1982) 818 (in Russian).
[19] E.I. Zenkevich, G.A. Kochubeev, A.P. Losev, G.P. Gurinovich, Molekulyarnaya Biologiya 12 (1978) 1002–1011 (in Russian).
[20] P.H. Hynninen, Acta Chem. Scand. B31 (1977) 829–835.
[21] P.H. Hynninen, S. Lötjönen, Synthesis 9 (1983) 705–708.
[22] A.P. Losev, V.N. Knyukshto, G.V. Gulhandanyan, J. Appl. Spectr. 58 (1993) 114 (in Russian).
[23] J.R. Lakowicz, in: Principles of Fluorescence Spectroscopy, Plenum Press, New York, 1983, pp. 120–123.
[24] M. Kasha, Pure and Appl. Chem. 11 (1965) 371–393.
[25] K. Ballschmiter, K. Truesdell, J.J. Katz, Biochim. Biophys. Acta 184 (1969) 604–613.
[26] M. van Gurp, G. van Ginkel, Y.K. Levine, Biochim. Biophys. Acta 973 (1989) 405–413.
[27] V. Sundström, T. Gillbro, R.A. Gadonas, A. Piskarskas, J. Chem. Phys. 89 (1988) 2754–2762.
[28] S. De Boer, D.A. Wiersma, Chem. Phys. Lett. 165 (1990) 45–53.
[29] G. Scheibe, in: W. Foerst (Ed.), Optische Angerungen organischer Systeme, Verlag Chemie, Weinheim, 1966, p. 109.
[30] T. Pullerits, F. van Mourik, R. Monshouwer, R.W. Visscher, R. van Grondelle, J. Lumin. 58 (1994) 168–171.
[31] C.R. Cantor, P.R. Schimmel, in: A.C. Bartlett, P.C. Vapnek, L.W. McCombs (Eds.), Biophysical Chemistry, Part II, W.H. Freeman, New York, 1980, pp. 390–398.
[32] D. Keller, C. Bustamante, J. Chem. Phys. 84 (1986) 2972–2980.
[33] V. Barzda, G. Garab, V. Gulbinas, L. Valkunas, Biochim. Biophys. Acta 1273 (1996) 231–236.
[34] R.P. Lehmann, R.A. Brunisholz, H. Zuber, Photosynth. Res. 41 (1994) 165–173.
[35] V. Barzda, L. Mustardy, G. Garab, Biochemistry 33 (1994) 10837–10841.